

Temperature-induced valence-state transition in double perovskite $\text{Ba}_{2-x}\text{Sr}_x\text{TbIrO}_6$

Z. Y. Zhao,^{1,2,3} S. Calder,⁴ M. H. Upton,⁵ H. D. Zhou,² Z. Z. He,³ M. A. McGuire,¹ and J.-Q. Yan¹

¹*Materials Science and Technology Division, Oak Ridge National Laboratory, Oak Ridge, Tennessee 37831, USA*

²*Department of Physics and Astronomy, University of Tennessee, Knoxville, Tennessee 37996, USA*

³*State Key Laboratory of Structural Chemistry, Fujian Institute of Research on the Structure of Matter, Chinese Academy of Sciences, Fuzhou, Fujian 350002, People's Republic of China*

⁴*Neutron Scattering Division, Oak Ridge National Laboratory, Oak Ridge, Tennessee 37831, USA*

⁵*X-ray Science Division, Argonne National Laboratory, Argonne, Illinois 60439, USA*

(Dated: May 5, 2022)

In this work, a temperature-induced valence-state transition is studied in a narrow composition range of $\text{Ba}_{2-x}\text{Sr}_x\text{TbIrO}_6$ by means of x-ray and neutron powder diffraction, resonant inelastic x-ray scattering, magnetic susceptibility, electrical resistivity, and specific heat measurements. The valence-state transition involves an electron transfer between Tb and Ir leading to the valence-state change between $\text{Tb}^{3+}/\text{Ir}^{5+}$ and $\text{Tb}^{4+}/\text{Ir}^{4+}$ phases. This first-order transition has a dramatic effect on the lattice, transport properties, and the long-range magnetic order at low temperatures for both Tb and Ir ions. Ir^{5+} ion has an electronic configuration of $5d^4$ ($J_{\text{eff}} = 0$) which is expected to be nonmagnetic. In contrast, Ir^{4+} ion with a configuration of $5d^5$ ($J_{\text{eff}} = 1/2$) favors a long-range magnetic order. For $x = 0.1$ with $\text{Tb}^{3+}/\text{Ir}^{5+}$ configuration to the lowest temperature (2 K) investigated in this work, a spin-glass behavior is observed around 5 K indicating Ir^{5+} ($J_{\text{eff}} = 0$) ions act as a spacer reducing the magnetic interactions between Tb^{3+} ions. For $x = 0.5$ with $\text{Tb}^{4+}/\text{Ir}^{4+}$ configuration below the highest temperature 400 K of this work, a long-range antiferromagnetic order at $T_N = 40$ K is observed highlighting the importance of Ir^{4+} ($J_{\text{eff}} = 1/2$) ions in promoting the long-range magnetic order of both Tb and Ir ions. For $0.2 \leq x \leq 0.375$, a temperature-induced valence-state transition from high-temperature $\text{Tb}^{3+}/\text{Ir}^{5+}$ phase to low-temperature $\text{Tb}^{4+}/\text{Ir}^{4+}$ phase occurs in the temperature range $180 \text{ K} \leq T \leq 325 \text{ K}$ and the transition temperature increases with x . The compositional dependence demonstrates the ability to tune the the valence state for a critical region of x that leads to a concurrent change in magnetism and structure. This tuning ability could be employed with suitable strain in thin films to act as a switch as the magnetism is manipulated.

INTRODUCTION

The complex interplay among spin-orbit coupling (SOC), on-site Coulomb interaction, non-cubic crystal field, and electronic bandwidths leads to rich exotic phenomena and novel physics in $4d/5d$ transition-metal compounds [1–3]. One important manifestation is the non-trivial $J_{\text{eff}} = 1/2$ Mott state in Sr_2IrO_4 with tetravalent Ir^{4+} ($5d^5$) ions, in which the lower $J_{\text{eff}} = 3/2$ band is fully occupied leaving the higher $J_{\text{eff}} = 1/2$ band half filled, see Fig. 1(a) [4]. Such spin-orbit-entangled $J_{\text{eff}} = 1/2$ scenario can give rise to unique magnetic ground states in $4d^5$ and $5d^5$ compounds, such as Kitaev quantum spin liquid [5]. Compounds containing transition-metal ions with $4d^3$ or $5d^3$ configuration can host magnetism with magnetic ordering temperatures even above room temperature [6–10]. In contrast to the rich magnetic phenomena for $4d/5d$ ions with 3 or 5 electrons, a nonmagnetic state is expected for $J_{\text{eff}} = 0$ compounds in which $5d$ transition-metal ions have four electrons that are paired in $J_{\text{eff}} = 3/2$ band, see Fig. 1(b). Despite the theoretical prediction of excitonic magnetism and tremendous experimental efforts, the search for an intrinsic long-range magnetic order in $J_{\text{eff}} = 0$ compounds is still ongoing [11–31]. One challenge is to distinguish the magnetism from lattice defects or unintentional doping.

The preference of a nonmagnetic ground state for d^4 ions indicates possible switch on/off of magnetism by controlling the charge transfer between d^4 and d^3 or d^5 ions. One approach toward this magnetism control is intermetallic charge transfer driven by temperature, chemical or hydrostatic pressure, or other external stimuli such as electric or magnetic fields. The intermetallic charge transfer is quite rare in transition-metal oxides [32]. However, rare-earth ions Pr, Ce, Tb can stabilize in different oxidation states in perovskite structured oxides which makes possible charge transfer between these rare-earth and transition-metal ions. One good example of such an intermetallic charge transfer is $(\text{Pr}, \text{Y})_{1-x}\text{Ca}_x\text{CoO}_3$ in which the charge transfer from Pr to Co ions at low temperatures changes the valence state of both Pr and Co ions and induces a metal-insulator transition accompanied with magnetic and structural anomalies [33].

A similar charge transfer was also reported in $\text{Sr}_2\text{TbRu}_{1-x}\text{Ir}_x\text{O}_6$ [34, 35] and $\text{Ba}_2\text{PrRu}_{1-x}\text{Ir}_x\text{O}_6$ [36, 37] where the chemical pressure from mixing Ru and Ir induces a charge transfer between the rare-earth and transition-metal ions. This first-order valence-state transition induces a sudden change of lattice and magnetic properties. The effect of $J_{\text{eff}} = 0$ ions and valence state change on the magnetic properties is well illustrated by the evolution of magnetic properties with Ir substitution in $\text{Sr}_2\text{TbRu}_{1-x}\text{Ir}_x\text{O}_6$ [35]. $\text{Sr}_2\text{Tb}^{3+}\text{Ru}^{5+}\text{O}_6$ shows

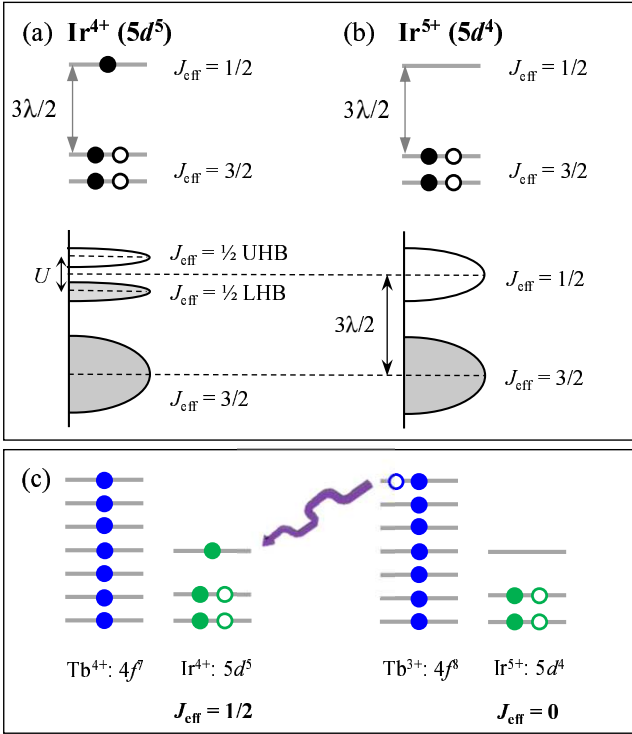


FIG. 1. (Color online) (a, b) Schematic diagrams of electron filling on t_{2g} level split by spin-orbit coupling (SOC) for Ir⁴⁺ (5d⁵) and Ir⁵⁺ (5d⁴) configurations. λ is the strength of SOC, U is the on-site Coulomb interaction. (c) Electronic configuration of Tb⁴⁺/Ir⁴⁺ and Tb³⁺/Ir⁵⁺. The arrow illustrates the electron transfer from Tb to Ir leading to the valence-state transition.

a long-range magnetic order at 41 K. With increasing substitution of Ru⁵⁺ (4d³) by $J_{\text{eff}} = 0$ Ir⁵⁺ (5d⁴) ions, the magnetic order is suppressed and disappeared around $x = 0.8$. With $x \geq 0.85$, the chemical pressure leads to the transfer of one electron from Tb³⁺ to Ru⁵⁺/Ir⁵⁺ site resulting in Sr₂Tb⁴⁺(Ru_{1-x}Ir_x)⁴⁺O₆ ordered around 50 K. This compositional dependence suggests the nonmagnetic nature of 5d⁴ Ir⁵⁺ ($J_{\text{eff}} = 0$) and highlights the importance of 5d⁵ Ir⁴⁺ ($J_{\text{eff}} = 1/2$) in the long-range magnetic order of both rare-earth and transition-metal ions in this system.

Mixing Ba and Sr without disturbing the transition-metal site in Ba_{2-x}Sr_xTbIrO₆ was proposed to induce a valence-state transition, which has been studied from the structural point of view at room temperature [38]. Ba₂Tb³⁺Ir⁵⁺O₆ ($x = 0$) crystallizes in a cubic structure with a $Fm\bar{3}m$ space group (see Fig. 2(a)) and paramagnetic down to 2 K [39], while Sr₂Tb⁴⁺Ir⁴⁺O₆ ($x = 2$) crystallizes in a monoclinic structure with a $P2_1/n$ space group (see Fig. 2(a)) and undergoes two antiferromagnetic (AFM) transitions at 51 K and 25 K [40, 41]. On account of the smaller size of Sr cations, the lower tolerance factor (0.992 for Ba₂TbIrO₆ [39] and 0.959 for Sr₂IrO₆ [41]) induces the tilting and distortion of the TbO₆/IrO₆

octahedra and SrO₁₂ polyhedra, which is responsible for the change of the crystal structure from cubic to monoclinic. With increasing x in Ba_{2-x}Sr_xTbIrO₆, the lattice parameter shows a sudden drop around $x = 0.35$ suggesting a valence-state change from Tb³⁺/Ir⁵⁺ to Tb⁴⁺/Ir⁴⁺ phase.

Because the ionic radius of Sr²⁺ is smaller than that of Ba²⁺, partial substitution of Ba²⁺ by Sr²⁺ is expected to reduce the tolerance factor, which measures the stability and distortion of perovskites. The transition from Tb³⁺/Ir⁵⁺ to Tb⁴⁺/Ir⁴⁺ phase with increasing x in Ba_{2-x}Sr_xTbIrO₆ signals that a smaller tolerance factor stabilizes the Tb⁴⁺/Ir⁴⁺ phase. For most perovskites, the tolerance factor has a positive temperature dependence. This indicates that Ba_{2-x}Sr_xTbIrO₆ members near the critical composition $x = 0.35$ can have a temperature-induced valence-state transition between the high-temperature Tb³⁺/Ir⁵⁺ and the low-temperature Tb⁴⁺/Ir⁴⁺ configurations, which hasn't been studied yet. More importantly, the valence-state transition can have a dramatic effect on the magnetic properties considering the change of the electronic configuration of Ir and might be employed to tune magnetism, as shown in Fig. 1(c). In this work, we investigate the thermally-driven valence-state transition in Ba_{2-x}Sr_xTbIrO₆ with the motivation of understanding its effect on the low-temperature magnetism and possible switchable magnetism using the transition between $J_{\text{eff}} = 0$ and $J_{\text{eff}} = 1/2$ at Ir site. The thermally-driven valence-state transition was investigated in the composition range $0.2 \leq x \leq 0.375$ by measuring x-ray and neutron powder diffraction, resonant inelastic x-ray scattering, magnetic susceptibility, electrical resistivity, and specific heat. The valence-state transition has a dramatic effect on the electronic configuration of Ir and thus the long-range magnetic order at low temperatures for both Tb and Ir ions. A magnetic order is observed in Ba_{2-x}Sr_xTb⁴⁺Ir⁴⁺O₆ but absent in Ba_{2-x}Sr_xTb³⁺Ir⁵⁺O₆. The valence-state change is associated with a dramatic first-order structural change of the lattice. Consequently, control of the lattice, through strain or pressure, is a potential route to further control and drive the valence state and associated magnetic order. This would yield a switchable mechanism to turn on and off the magnetism which deserves further investigation.

EXPERIMENTS

Polycrystalline Ba_{2-x}Sr_xTbIrO₆ samples ($x = 0, 0.1, 0.2, 0.325, 0.35, 0.375, 0.4, 0.5, \text{ and } 2$) were synthesized by the solid state reaction method. BaCO₃, SrCO₃, Tb₄O₇, and IrO₂ were used as starting materials. The stoichiometric and homogeneous mixture was pelletized and fired from 1000°C to 1200°C for up to 6 days with intervening regrindings and repelletizings.

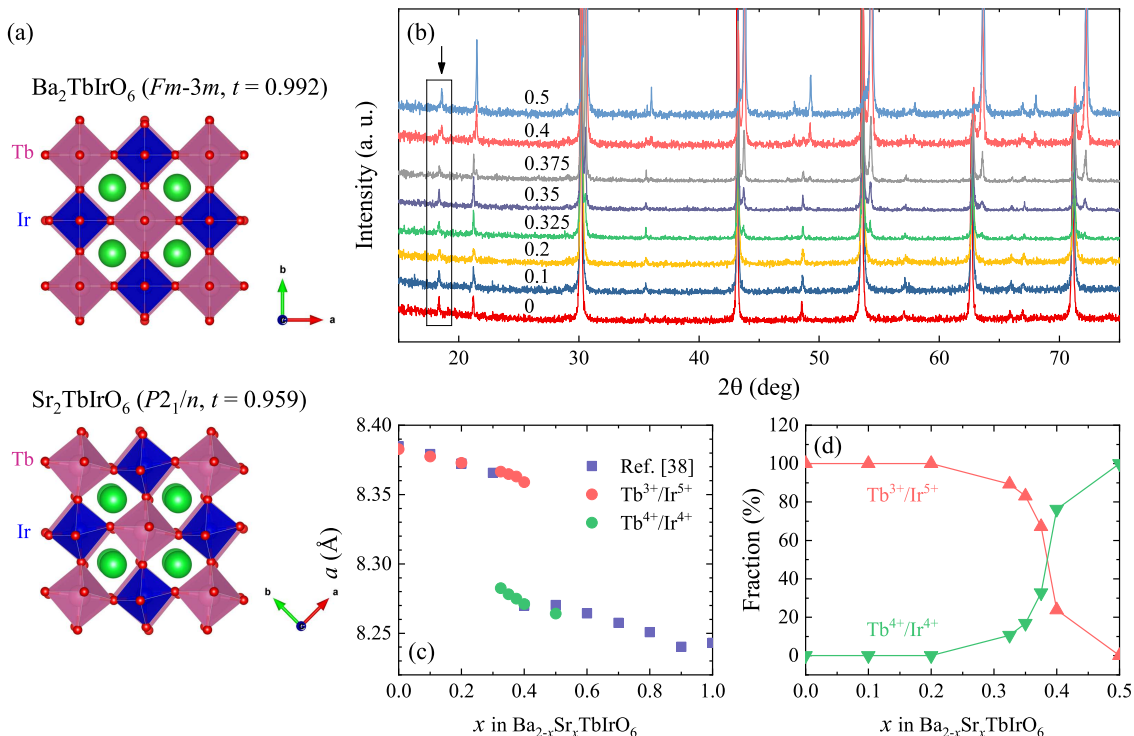


FIG. 2. (Color online) (a) Crystal structures of $\text{Ba}_2\text{TbIrO}_6$ and $\text{Sr}_2\text{TbIrO}_6$ projected in the ab plane. The space group and tolerance factor t are also given. (b) Powder x-ray diffraction patterns of $\text{Ba}_{2-x}\text{Sr}_x\text{TbIrO}_6$ collected at room temperature. The superlattice indicating the ordered arrangement of Tb and Ir cations is highlighted by the rectangle. (c) Composition dependence of the refined lattice parameters. The lattice parameters reported in Ref. [38] are also given for comparison. In the composition range plotted, both the $\text{Ba}_{2-x}\text{Sr}_x\text{Tb}^{3+}\text{Ir}^{5+}\text{O}_6$ and $\text{Ba}_{2-x}\text{Sr}_x\text{Tb}^{4+}\text{Ir}^{4+}\text{O}_6$ phases are cubic with a space group $Fm-3m$. (d) Evolution with x of the fraction of $\text{Ba}_{2-x}\text{Sr}_x\text{Tb}^{3+}\text{Ir}^{5+}\text{O}_6$ and $\text{Ba}_{2-x}\text{Sr}_x\text{Tb}^{4+}\text{Ir}^{4+}\text{O}_6$ determined from the Rietveld refinements.

Powder x-ray diffraction (XRD) was carried out on a PANalytical X'Pert Pro MPD powder x-ray diffractometer using $\text{Cu } K_{\alpha 1}$ radiation. Room-temperature diffractions for all compositions were performed in the range $10^\circ \leq 2\theta \leq 90^\circ$. Variable temperature XRD for $x = 0.2$ was collected between 52.5° and 55.5° down to 20 K using an Oxford PheniX closed cycle cryostat.

Magnetic susceptibility (χ) was measured in the temperature range $2 \text{ K} \leq T \leq 380 \text{ K}$ on a Magnetic Property Measurement System (Quantum Design, QD). Specific heat (C_p) was measured by the relaxation method between 2 K and 300 K using a QD Physical Property Measurement System (PPMS). Electrical resistivity (ρ) was also measured between 100 K and 380 K on the PPMS.

Neutron powder diffraction was performed on the HB-2A Powder diffractometer at the High Flux Isotope Reactor, Oak Ridge National Laboratory. The sample was contained in an annular Al sample holder to reduce the absorption from Ir. Diffraction patterns were collected from 1.5 K to 60 K in a helium cryostat. A wavelength of 2.41 \AA was selected from a vertically focusing germanium monochromator from the Ge113 reflection.

Resonant Inelastic x-ray Scattering (RIXS) was performed on the MERIX beamline, 27-ID, at the Advanced

Photon Source, Argonne National Laboratory. The finely ground powder samples were contained in a custom Al sample holder with Kapton windows for the three compositions of $x = 0.1, 0.2, 2.0$. The incident energy was tuned to the Ir L_3 -edge (11.215 keV) resonant edge to enhance the Ir scattering. The inelastic energy was measured with the use of a Si(844) analyzer. The energy resolution was determined to be 35 meV at full width half maximum, based on fitting the quasi-elastic line to a charge peak. The scattering plane and incident photon polarization were both horizontal, i.e. π incident polarization, with the incident beam focused to a size of $40 \times 25 \text{ microns}^2$ ($\text{H} \times \text{V}$) at the sample position. To minimize the elastic scattering, measurements were performed with 2θ at 90° in horizontal geometry. Temperature dependent measurements were collected from 5 K to 295 K using a closed cycle refrigerator.

RESULTS AND DISCUSSIONS

Valence-state transition in $\text{Ba}_{2-x}\text{Sr}_x\text{TbIrO}_6$ from room-temperature XRD

Figure 2(b) shows the powder XRD patterns of $\text{Ba}_{2-x}\text{Sr}_x\text{TbIrO}_6$ ($0 \leq x \leq 0.5$) collected at room temperature. All these samples were fired in air at 1200°C for 48 hours. The existence of the superlattice reflection for all compositions at $2\theta \approx 19^\circ$ indicates an ordered arrangement of Tb and Ir ions. For $x = 0$, the Rietveld refinement (see Fig. S1 in Supplemental Materials) confirms the cubic structure, and the lattice parameters agree well with previous reports of $\text{Ba}_{2-x}\text{Sr}_x\text{Tb}^{3+}\text{Ir}^{5+}\text{O}_6$ [38]. With increasing Sr concentration, extra reflections are observed above $x = 0.325$. These extra reflections can also be indexed with the cubic $Fm\bar{3}m$ structure but with a smaller lattice parameter. According to Refs. [38, 39], this new cubic phase is $\text{Ba}_{2-x}\text{Sr}_x\text{Tb}^{4+}\text{Ir}^{4+}\text{O}_6$. The intensity of those reflections from $\text{Tb}^{4+}/\text{Ir}^{4+}$ increases with more Sr substitution. Figure 2(c) shows the evolution with Sr content of the room temperature lattice parameters. Also plotted are the data from Ref. [38], and the results agree well. With increasing x , the lattice parameter gradually decreases and shows a sudden drop around $x_c = 0.325$, which corresponds to the valence-state transition with electron configuration from $\text{Tb}^{3+}/\text{Ir}^{5+}$ to $\text{Tb}^{4+}/\text{Ir}^{4+}$ state. From room temperature powder XRD patterns, these two cubic phases co-exist in the composition range $0.325 \leq x \leq 0.4$. Figure 2(d) shows how Sr content affects the fractions of the $\text{Tb}^{3+}/\text{Ir}^{5+}$ and $\text{Tb}^{4+}/\text{Ir}^{4+}$ phases in $\text{Ba}_{2-x}\text{Sr}_x\text{TbIrO}_6$. The fraction of the $\text{Tb}^{4+}/\text{Ir}^{4+}$ phase is dramatically enhanced in $x = 0.4$ with only a few percentage of residual $\text{Tb}^{3+}/\text{Ir}^{5+}$ phase.

We noticed that the fraction of these two cubic phases depends on the sintering conditions. For example, for $x = 0.35$, about 17%wt of $\text{Tb}^{4+}/\text{Ir}^{4+}$ phase was found when the pellet was fired at 1200°C for 48 hours. This fraction increases to 33%wt when fired at 1250°C for 48 hours or at 1200°C for 144 hours (see Fig. S2 in Supporting Materials for details). This processing dependence might be related to variation of Ir deficiency and/or the oxygen content in the sample after an extended sintering.

Temperature-induced valence-state transition in $\text{Ba}_{1.8}\text{Sr}_{0.2}\text{TbIrO}_6$

The above room-temperature XRD studies show that the doping-induced valence-state transition occurs in a narrow composition range around $x_c = 0.325$. As explained in the Introduction, one would expect a thermally driven valence-state transition near $x_c = 0.325$ considering the temperature dependence of the tolerance factor for most perovskites. To verify this, we investigated

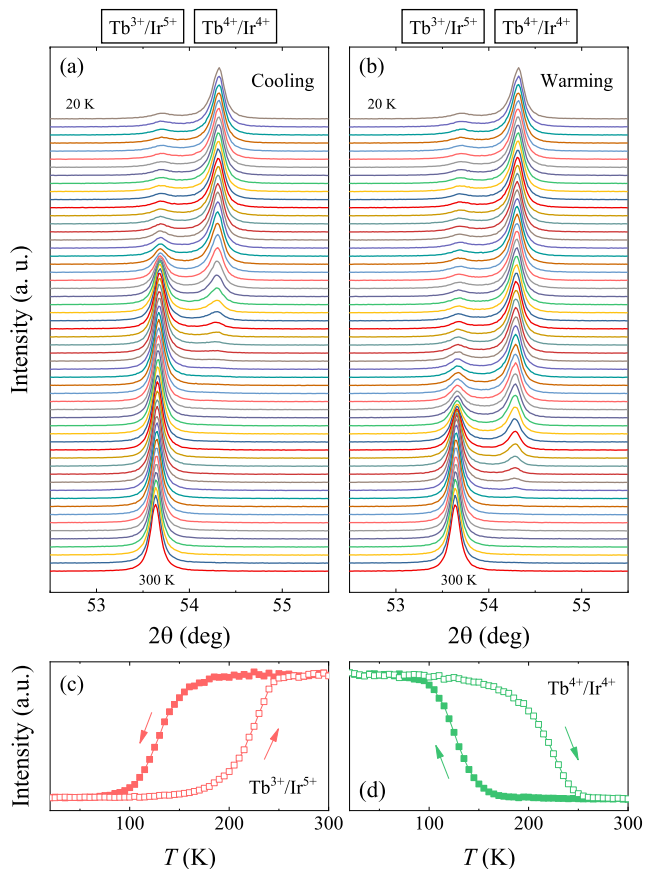


FIG. 3. (Color online) Evolution with temperature of the cubic (422) peak for $x = 0.2$ monitored upon (a) cooling and (b) warming in the temperature range $20 \text{ K} \leq T \leq 300 \text{ K}$. The arrows denote the direction of sweeping temperature. (c, d) Temperature dependencies of the (422) peak intensity for $\text{Tb}^{3+}/\text{Ir}^{5+}$ and $\text{Tb}^{4+}/\text{Ir}^{4+}$ phase, respectively.

the structure, valence state of Ir, magnetic and transport properties, magnetic structure of $\text{Ba}_{1.8}\text{Sr}_{0.2}\text{TbIrO}_6$ by measuring low-temperature x-ray and neutron powder diffraction, RIXS, magnetic susceptibility, and electrical resistivity. This composition is particularly investigated because it is single phase at room temperature as shown in Fig. 2. Therefore, the appearance of the $\text{Tb}^{4+}/\text{Ir}^{4+}$ phase or the valence-state transition could be better resolved upon cooling.

Low-temperature XRD — The variable-temperature powder XRD patterns were recorded down to 20 K. Figures 3(a, b) show the evolution with temperature of the (422) reflection upon cooling and warming, respectively. At 300 K, one single peak is observed at $2\theta \approx 53.6^\circ$, suggesting that the sample has a single $\text{Tb}^{3+}/\text{Ir}^{5+}$ phase. With decreasing temperature, a weak peak centering around $2\theta \approx 54.3^\circ$, which is the (422) reflection of the $\text{Tb}^{4+}/\text{Ir}^{4+}$ phase, starts to appear below $T_{v,\downarrow} = 150 \text{ K}$, as seen in Fig. 3(a). The peak intensity of $\text{Tb}^{4+}/\text{Ir}^{4+}$ phase increases upon further cooling, while the peak intensity

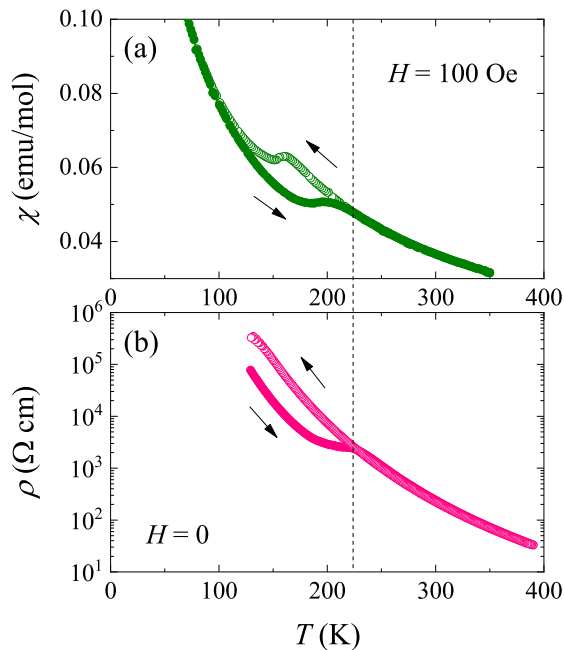


FIG. 4. (Color online) Temperature dependence of (a) magnetic susceptibility and (b) electrical resistivity for $x = 0.2$ measured upon warming and cooling as marked by arrows.

of $\text{Tb}^{3+}/\text{Ir}^{5+}$ phase decreases. After dwelling at 20 K for about one hour, the profile of these two peaks were monitored upon warming. The peak intensity of $\text{Tb}^{4+}/\text{Ir}^{4+}$ phase starts to decrease around $T_{v,\uparrow} = 180$ K while that of $\text{Tb}^{3+}/\text{Ir}^{5+}$ phase starts to increase. Above about 250 K, only the $\text{Tb}^{3+}/\text{Ir}^{5+}$ phase is left. We also performed low-temperature x-ray powder diffraction measurements on $x = 0.1$ and 0.5. As shown in the Supporting Materials (Fig. S3), we did not observe similar dramatic change in peak intensity.

The appearance of the $\text{Tb}^{4+}/\text{Ir}^{4+}$ phase at lower temperatures provides a clear evidence for the temperature-induced valence-state transition from $\text{Tb}^{3+}/\text{Ir}^{5+}$ to $\text{Tb}^{4+}/\text{Ir}^{4+}$ configuration in $\text{Ba}_{1.8}\text{Sr}_{0.2}\text{TbIrO}_6$. The different transition temperatures $T_{v,\uparrow} \approx 180$ K and $T_{v,\downarrow} \approx 150$ K indicate a first-order nature of this transition. The transition is not complete at 20 K, leading to a mixed-phase state due to the polycrystalline nature of our samples.

Magnetic and transport response to the valence-state transition — The magnetic susceptibility, $\chi(T)$, as a function of temperature measured in an applied field of 100 Oe is shown in Fig. 4(a). Upon cooling, $\chi(T)$ shows a step-like change around 170 K. While upon warming, the change occurs around 200 K. The obvious hysteresis in $\chi(T)$ is consistent with that observed in low temperature XRD measurements and is a clear evidence for the first-order nature of this valence-state transition. A Curie-Weiss fitting of the magnetic susceptibility above 200 K gives an effective moment of $9.70 \mu_B$ and a Weiss

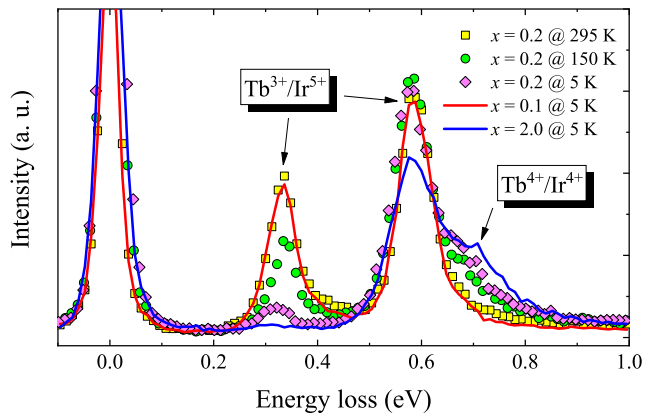


FIG. 5. (Color online) RIXS spectra as a function of energy loss measured for $x = 0.2$. Data collected on $x = 0.1$ and $x = 2$ are used as a reference for $\text{Tb}^{3+}/\text{Ir}^{5+}$ and $\text{Tb}^{4+}/\text{Ir}^{4+}$ configurations, respectively.

constant of -21 K. The effective moment is as expected for Tb^{3+} and similar to that of $x = 0.1$ presented later.

Figure 4(b) shows the temperature dependence of the electrical resistivity, $\rho(T)$. A resistive behaviour is observed below 400 K. Upon cooling, $\rho(T)$ increases from about $20 \Omega\text{cm}$ at 400 K to $3 \times 10^5 \Omega\text{cm}$ at 130 K, below which the sample is too resistive for any reliable data from our machine. When measured on warming, $\rho(T)$ exhibits a kink around 220 K, where the hysteresis in $\chi(T)$ occurs. We also measured $\rho(T)$ for $x = 0.1$ and 0.5 where no valence-state transition is expected (data not shown). We did not see any anomaly as observed in Fig. 4(b).

Resonant inelastic x-ray scattering — To verify that the above anomalies in the low-temperature XRD study is indeed from the transition between $\text{Tb}^{3+}/\text{Ir}^{5+}$ and $\text{Tb}^{4+}/\text{Ir}^{4+}$ phases due to the charge transfer between Tb and Ir ions, we measured RIXS for three $\text{Ba}_{2-x}\text{Sr}_x\text{TbIrO}_6$ samples with $x = 0.1, 0.2,$ and 2. RIXS is element specific and measures directly transitions between $d-d$ orbitals; therefore, it is a powerful probe to provide direct information on the valence states of the Ir ions in this compound [42]. At 295 K, as shown in Fig. 5, the spectrum for $x = 0.2$ exhibits two peaks around 0.3 and 0.6 eV. At lower temperatures, two features are observed: (i) the intensity of the high-energy peak is nearly temperature independent while the low-energy peak is significantly suppressed; (ii) a shoulder around 0.7 eV gradually arises. To explain the evolution of the peak intensity with temperature, the RIXS spectra of $x = 0.1$ and 2 are also plotted as a reference. At 295 K, the spectrum of $x = 0.2$ matches well with the $x = 0.1$ curve, indicating a pure $\text{Tb}^{3+}/\text{Ir}^{5+}$ phase. At lower temperatures, the emergence of the shoulder feature indicates the presence of the $\text{Tb}^{4+}/\text{Ir}^{4+}$ phase, which is therefore a very direct evidence for the valence-state transition between $\text{Tb}^{3+}/\text{Ir}^{5+}$ and $\text{Tb}^{4+}/\text{Ir}^{4+}$ states. The weak but visible

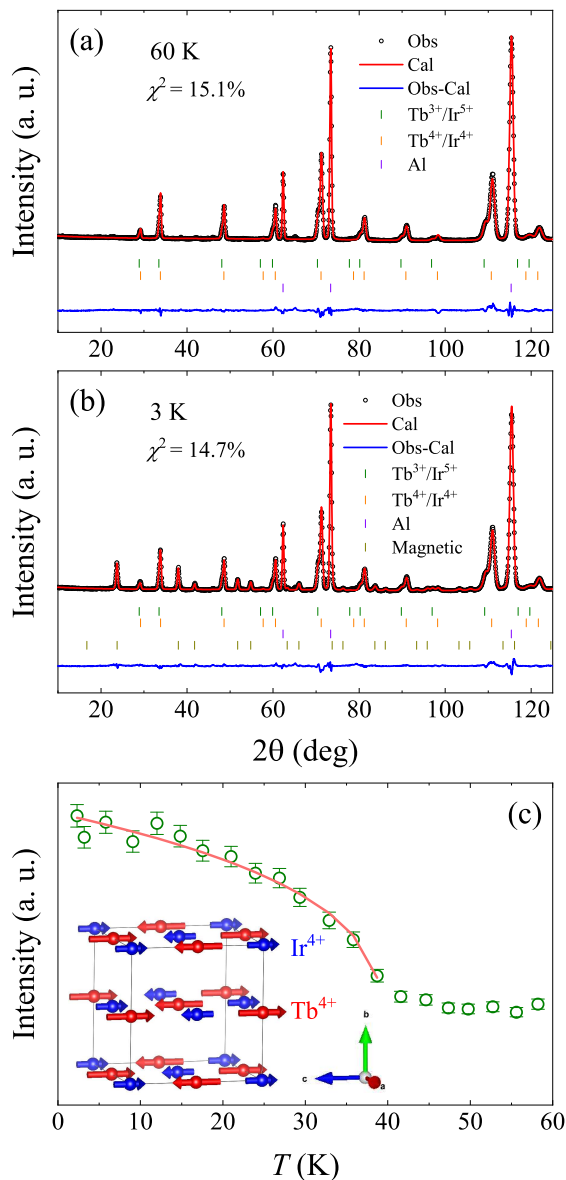


FIG. 6. (Color online) Neutron powder diffraction performed on $x = 0.2$ at (a) 60 K and (b) 3 K. In panel (a), the vertical-tick marks from top to bottom correspond to $\text{Tb}^{3+}/\text{Ir}^{5+}$ phase (green), $\text{Tb}^{4+}/\text{Ir}^{4+}$ phase (orange), and Al can (blue). The additional set of vertical tick marks in panel (b) at the bottom are the magnetic reflections. (c) Temperature dependence of the peak intensity around $2\theta = 23.8^\circ$. The solid line is a fit as described in the text. The inset is the arrangement of Tb^{4+} spins (red) and Ir^{4+} spins (blue).

low-energy peak for $x = 0.2$ at 5 K supports the phase coexistence as deduced from the variable-temperature XRD results.

Nuclear and magnetic structure from neutron powder diffraction— Figure 6(a) shows the Rietveld refinement of the neutron powder diffraction pattern for $x = 0.2$ collected at 60 K, which is consistent with the XRD result including both $\text{Tb}^{3+}/\text{Ir}^{5+}$ and $\text{Tb}^{4+}/\text{Ir}^{4+}$ phases below

T_c . The respective lattice parameter is $a = 8.3423(5)$ Å for the $\text{Tb}^{3+}/\text{Ir}^{5+}$ phase and $a = 8.2680(2)$ Å for the $\text{Tb}^{4+}/\text{Ir}^{4+}$ phase. Some extra strong reflections are observed at 3 K in Fig. 6(b). The d -spacing proves that this set of magnetic peaks come from the $\text{Tb}^{4+}/\text{Ir}^{4+}$ phase. Figure 6(c) shows the temperature dependence of the peak intensity at $2\theta = 23.8^\circ$, which confirms the long-range magnetic order at 40 K. The positions of the magnetic reflections are compatible with a propagation vector $\mathbf{k} = (0, 0, 1)$. A representational analysis approach was utilized with the aid of the SARAH program [44]. For a propagation vector $\mathbf{k} = (0, 0, 1)$ and magnetic Tb ions at $(0.5, 0.5, 0.5)$ and Ir ions at $(0, 0, 0)$ in the $Fm\bar{3}m$ space group, there are two symmetry allowed irreducible representations: Γ_3 and Γ_9 in Kovalevs scheme. Γ_9 confines the spins on both Ir and Tb ions to the c axis and was found to provide the best fit to the data. Any determination of canting away from the c axis is beyond the limits of the data. As illustrated in the inset to Fig. 6(c), both the magnetic moments of the Tb^{4+} and Ir^{4+} spins are aligned along the c direction. The Tb^{4+} and Ir^{4+} sublattices couple ferromagnetically in the ab plane, which are further arranged antiferromagnetically along the c direction. The deduced magnetic moment is about $5.98(4) \mu_B$ for Tb^{4+} ion and $0.5(1) \mu_B$ for Ir^{4+} ion. It should be noted that the low signal from Ir makes accurate isolation of the signal challenging and these values are best fits only.

The coexistence of the $\text{Tb}^{3+}/\text{Ir}^{5+}$ and $\text{Tb}^{4+}/\text{Ir}^{4+}$ phases with a reasonable phase fraction allows us to obtain the structural parameters of each phase from Rietveld refinement of the neutron powder diffraction patterns collected at different temperatures. As shown in Table I, the $\text{Tb}^{4+}/\text{Ir}^{4+}$ phase has a smaller lattice parameter than the $\text{Tb}^{3+}/\text{Ir}^{5+}$ phase. This is consistent with that determined by x-ray powder diffraction. The $\text{Tb}^{4+}/\text{Ir}^{4+}$ phase has an elongated Ir-O bond but shortened Ba-O and Tb-O bonds compared to the $\text{Tb}^{3+}/\text{Ir}^{5+}$ phase. Also shown in Table I are the oxidation states of Tb and Ir estimated from bond valence sum, which in general agree with the expected oxidation states of Tb and Ir ions in each phase.

Evolution with x of the valence-state transition and low-temperature magnetic order of $\text{Ba}_{2-x}\text{Sr}_x\text{TbIrO}_6$

In order to understand how the valence-state transition evolves with the chemical pressure, we measured $\chi(T)$ curves of six different $\text{Ba}_{2-x}\text{Sr}_x\text{TbIrO}_6$ samples with $0.1 \leq x \leq 0.5$. Figures 7(a-e) show the $\chi(T)$ data below 100 K. For $x = 0.1$, $\chi(T)$ increases upon cooling and exhibits a slope change around 5 K, below which $\chi(T)$ measured in field-cooling (FC) mode starts to diverge from that collected in zero-field-cooling (ZFC). For $x = 0.5$, the slope change is absent but a kink at 40 K can be well resolved.

TABLE I. Structural parameters of $\text{Ba}_{2-x}\text{Sr}_x\text{TbIrO}_6$ ($x = 0.2$) at different temperatures obtained from Rietveld refinement of neutron powder diffraction patterns. The coexistence of the $\text{Tb}^{3+}/\text{Ir}^{5+}$ and $\text{Tb}^{4+}/\text{Ir}^{4+}$ phases with a reasonable phase fraction allows us to extract the structural parameters of each phase. The space group is $Fm-3m$ for both phases. The position of oxygen ($x, 0, 0$) is presented. Refinement of the Ba/Sr ratio found agreement with the nominal composition. The refinement also suggests a stoichiometric amount of oxygen. The oxidation states of Tb and Ir estimated from bond valence sum (BVS) are also shown. For the BVS calculation[43], Tb^{4+} , $R_0=2.018\text{\AA}$ and $B=0.395$. For Ir^{4+} , $R_0=1.909\text{\AA}$ and $B=0.258$.

	$\text{Tb}^{3+}/\text{Ir}^{5+}$ phase			$\text{Tb}^{4+}/\text{Ir}^{4+}$ phase		
	250 K	165 K	60 K	250 K	165 K	60 K
a (\AA)	8.3754(2)	8.3737(2)	8.3715(3)	8.2920(2)	8.2885(2)	
x_{O}	0.2344(2)	0.2328(4)	0.2329(6)	0.2407(3)	0.2412(3)	
Ba/Sr-O (\AA)	2.96402(10)	2.96405(18)	2.9632(3)	2.93268(10)	2.93132(10)	
Tb-O (\AA)	2.2245(17)	2.237(4)	2.236(6)	2.150(3)	2.145(3)	
BVS Tb^{4+}	3.56	3.45	3.46	4.30	4.35	
Ir-O (\AA)	1.9632(17)	1.949(4)	1.950(6)	1.996(3)	1.999(3)	
BVS Ir^{4+}	4.86	5.14	5.12	4.28	4.23	
$\angle\text{Tb-O-Ir}$ (deg)	180	180	180	180	180	
Fraction	100%	34.7(4)%	22.8(3)%	65.3(6)%	77.2%	

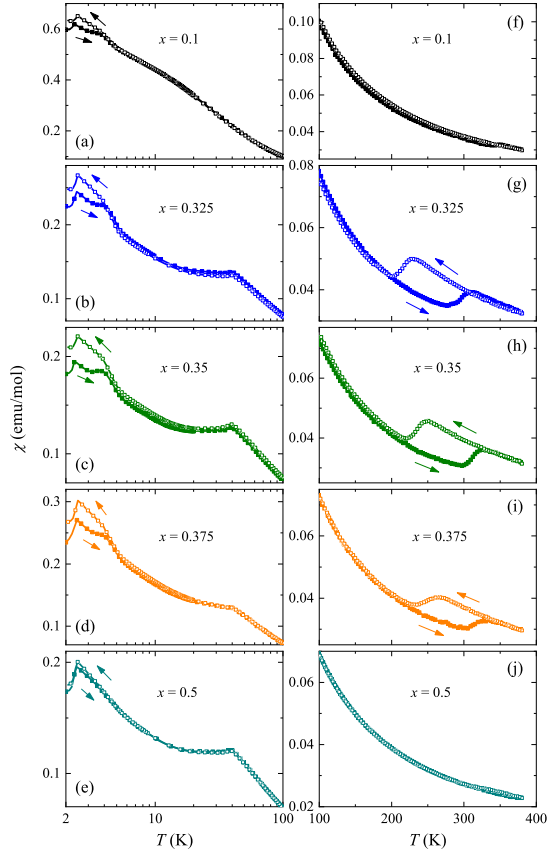


FIG. 7. (Color online) Temperature dependence of magnetic susceptibility for $\text{Ba}_{2-x}\text{Sr}_x\text{TbIrO}_6$ series measured in $H = 100$ Oe. $x = 0.5$ sample was measured in 500 Oe. Panels (a-f) highlight the features at low temperatures. The magnetic susceptibility of $x = 0.20$ is similar to that of $x = 0.325$ shown in panel (b). Panels (g-l) highlight the valence-state transition at high temperatures. Solid (open) symbols are measured in ZFC (FC) process. The drop of the magnetic susceptibility near 3 K comes from a small amount of Tb_2O_3 impurity.

For other compositions, both the slope change around 5 K and the kink around 40 K are present. A sudden drop of $\chi(T)$ upon cooling across ≈ 2.5 K is observed in all compositions and comes from a small amount of Tb_2O_3 impurity [45] that can barely be observed by room temperature x-ray powder diffraction. At high temperatures, see Figs. 7(f-j), a paramagnetic behavior is observed for $x = 0.1$ and 0.5 up to 380 K, while a clear first-order transition is observed for $0.2 \leq x \leq 0.375$ in the temperature range $180 \text{ K} \leq T \leq 320 \text{ K}$. The valence-state transition shifts to higher temperatures with increasing x . A Curie-Weiss fitting of the high-temperature magnetic susceptibility for $x = 0.1$ gives an effective moment of $9.74 \mu_B$ and a Weiss constant of -16 K . This effective moment is as expected for Tb^{3+} ions and confirms the $\text{Tb}^{3+}/\text{Ir}^{5+}$ state for $x = 0.1$. The Curie-Weiss fitting of $x = 0.5$ gives an effective moment of $8.47 \mu_B$ and a Weiss constant of -30 K . This effective moment is slightly larger than the expected value of $8.13 \mu_B$ for $\text{Tb}^{4+}/\text{Ir}^{4+}$ configuration.

The above complex temperature dependence of $\chi(T)$ shows a close relation between the high-temperature valence-state transition with the low-temperature magnetic order. For $x = 0.1$ with only $\text{Tb}^{3+}/\text{Ir}^{5+}$ phase, no long-range magnetic order is observed but a spin-glass state is developed below $\approx 5 \text{ K}$. For $x = 0.5$ with only $\text{Tb}^{4+}/\text{Ir}^{4+}$ phase, the kink feature around 40 K is a signature for the long-range AFM order. The absence of the splitting between FC and ZFC $\chi(T)$ indicates a collinear AFM spin arrangement as confirmed for the $\text{Tb}^{4+}/\text{Ir}^{4+}$ phase in $x = 0.2$ by the neutron diffraction measurements. For other compositions with a valence-state transition, the incomplete transition results in the coexistence of $\text{Tb}^{3+}/\text{Ir}^{5+}$ and $\text{Tb}^{4+}/\text{Ir}^{4+}$ phases. Therefore, both the slope change around 5 K and the kink around 40 K are observed in $\chi(T)$.

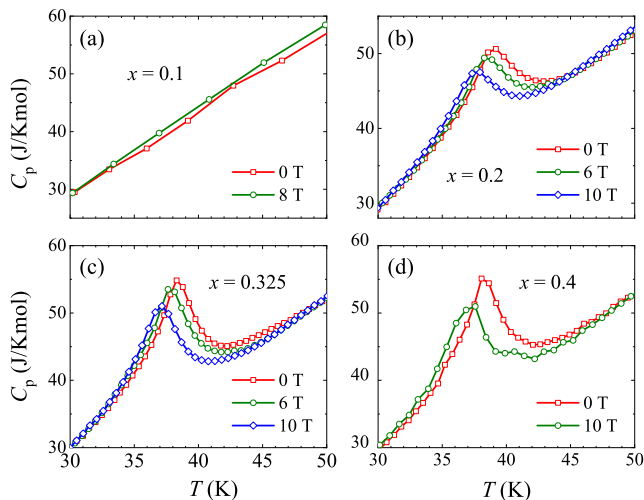


FIG. 8. (Color online) Specific heat of selected compositions of $\text{Ba}_{2-x}\text{Sr}_x\text{TbIrO}_6$.

The magnetic order around 40 K can be well resolved in the temperature dependence of specific heat as shown in Fig. 8. For $x = 0.1$, no anomaly is observed at either around 5 K or 40 K. The former is consistent with the spin-glass origin of the splitting of FC and ZFC curves; the latter confirms the absence of a long-range magnetic order. For other compositions, a λ -type anomaly due to the AFM order of the $\text{Tb}^{4+}/\text{Ir}^{4+}$ phase shows up near $T_N = 40$ K. Application of a magnetic field can suppress the magnetic order and reduce T_N .

SUMMARY

In summary, we study the temperature-induced valence-state transition in a narrow composition range $0.2 \leq x \leq 0.375$ in $\text{Ba}_{2-x}\text{Sr}_x\text{TbIrO}_6$. Upon cooling, one electron is transferred from Tb^{3+} to Ir^{5+} in the $\text{Ba}_{2-x}\text{Sr}_x\text{Tb}^{3+}\text{Ir}^{5+}\text{O}_6$ phase leading to the formation of the $\text{Ba}_{2-x}\text{Sr}_x\text{Tb}^{4+}\text{Ir}^{4+}\text{O}_6$ phase. No long-range magnetic order was observed in $\text{Ba}_{2-x}\text{Sr}_x\text{Tb}^{3+}\text{Ir}^{5+}\text{O}_6$ where the Ir^{5+} has an electronic configuration of $5d^4$ ($J_{\text{eff}} = 0$). The observation of the long-range magnetic order with $T_N = 40$ K in $\text{Ba}_{2-x}\text{Sr}_x\text{Tb}^{4+}\text{Ir}^{4+}\text{O}_6$, at which both Tb^{4+} and Ir^{4+} ions order simultaneously, suggests an essential role of Ir^{4+} ($J_{\text{eff}} = 1/2$) in mediating the magnetic interactions of Tb ions.

We noticed that the valence-state transition is not complete even at 2 K in our polycrystalline samples. Detailed studies on single crystals are desired to further understand the mechanism and effects of the valence-state transition. The first-order valence-state transition is sensitive to the chemical pressure induced by the size difference between Ba^{2+} and Sr^{2+} cations. It is thus reasonable to expect that strain field can be effective

in controlling the valence-state transition and thus the magnetism. This kind of effect can be better tested in thin films on different substrates or in-situ strain fields. Our results reported in this work show that the valence-state transition has a dramatic effect on the structure, magnetic and transport properties. Appropriate chemical doping that might induce electrical conductivity also deserves some efforts for novel phenomena accompanying with the valence-state transition.

ACKNOWLEDGEMENT

JQY would like to thank Nandini Trivedi, Patrick Woodward, and Jianshi Zhou for helpful discussions. Work at ORNL was supported by the US Department of Energy, Office of Science, Basic Energy Sciences, Materials Sciences and Engineering Division. Synthesis of powder samples for neutron diffraction measurement and part of the manuscript preparation by ZZ were supported by the National Natural Science Foundation of China (Grants No. U1832166 and 52072368). This research used resources at the High Flux Isotope Reactor, a DOE office of Science User Facility operated by the Oak Ridge National Laboratory. This research used resources of the Advanced Photon Source, a U.S. Department of Energy (DOE) Office of Science User Facility operated for the DOE Office of Science by Argonne National Laboratory under Contract No. DE-AC02-06CH11357.

REFERENCES

- [1] William Witczak-Krempa, Gang Chen, Yong Baek Kim, and Leon Balents, “Correlated quantum phenomena in the strong spin-orbit regime,” *Annu. Rev. Condens. Matter Phys.* **5**, 57–82 (2014).
- [2] Jeffrey G Rau, Eric Kin-Ho Lee, and Hae-Young Kee, “Spin-orbit physics giving rise to novel phases in correlated systems: Iridates and related materials,” *Annual Review of Condensed Matter Physics* **7**, 195–221 (2016).
- [3] Robert Schaffer, Eric Kin-Ho Lee, Bohm-Jung Yang, and Yong Baek Kim, “Recent progress on correlated electron systems with strong spin-orbit coupling,” *Reports on Progress in Physics* **79**, 094504 (2016).
- [4] BJ Kim, Hosub Jin, SJ Moon, J-Y Kim, B-G Park, CS Leem, Jaejun Yu, TW Noh, C Kim, S-J Oh, *et al.*, “Novel $j_{\text{eff}} = 1/2$ mott state induced by relativistic spin-orbit coupling in Sr_2IrO_4 ,” *Physical review letters* **101**, 076402 (2008).
- [5] Hidenori Takagi, Tomohiro Takayama, George Jackeli, Giniyat Khaliullin, and Stephen E Nagler, “Concept and realization of kitaev quantum spin liquids,” *Nature Reviews Physics* **1**, 264–280 (2019).

- [6] Walter Schnelle, Beluvalli E Prasad, Claudia Felser, Martin Jansen, Evgenia V Komleva, Sergey V Streltsov, Igor I Mazin, Dmitry Khalyavin, Pascal Manuel, Sukanya Pal, *et al.*, “Magnetic and electronic ordering phenomena in the Ru_2O_6 -layer honeycomb lattice compound $AgRuO_3$,” *Physical Review B* **103**, 214413 (2021).
- [7] Wei Tian, Chris Svoboda, M Ochi, M Matsuda, HB Cao, J-G Cheng, BC Sales, DG Mandrus, R Arita, Nandini Trivedi, *et al.*, “High antiferromagnetic transition temperature of the honeycomb compound $SrRu_2O_6$,” *Physical Review B* **92**, 100404 (2015).
- [8] CI Hiley, DO Scanlon, AA Sokol, SM Woodley, AM Ganose, S Sangiao, JM De Teresa, P Manuel, DD Khalyavin, M Walker, *et al.*, “Antiferromagnetism at $T_c = 500$ K in the layered hexagonal ruthenate $SrRu_2O_6$,” *Physical Review B* **92**, 104413 (2015).
- [9] YG Shi, YF Guo, S Yu, M Arai, AA Belik, A Sato, K Yamamura, E Takayama-Muromachi, HF Tian, HX Yang, *et al.*, “Continuous metal-insulator transition of the antiferromagnetic perovskite $NaOsO_3$,” *Physical Review B* **80**, 161104 (2009).
- [10] Efrain E Rodriguez, Frédéric Poineau, Anna Llobet, Brendan J Kennedy, Maxim Avdeev, Gordon J Thoroood, Melody L Carter, Ram Seshadri, David J Singh, and Anthony K Cheetham, “High temperature magnetic ordering in the d_4 perovskite $SrTiO_3$,” *Physical review letters* **106**, 067201 (2011).
- [11] Giniyat Khaliullin, “Excitonic magnetism in van Vleck-type d_4 Mott insulators,” *Physical review letters* **111**, 197201 (2013).
- [12] O Nganba Meetei, William S Cole, Mohit Randeria, and Nandini Trivedi, “Novel magnetic state in d_4 Mott insulators,” *Physical Review B* **91**, 054412 (2015).
- [13] Gang Cao, TF Qi, Li Li, Jsminka Terzic, SJ Yuan, Lance E DeLong, Ganpathy Murthy, and Ribhu K Kaul, “Novel magnetism of $Ir^{5+}(5d_4)$ ions in the double perovskite Sr_2IrO_6 ,” *Physical review letters* **112**, 056402 (2014).
- [14] Abhishek Nag, Srimanta Middey, Sayantika Bhowal, Swarup K Panda, Roland Mathieu, JC Orain, F Bert, P Mendels, Paul Gregory Freeman, M Mansson, *et al.*, “Origin of the spin-orbital liquid state in a nearly $j = 0$ iridate $Ba_3Zr_2O_9$,” *Physical review letters* **116**, 097205 (2016).
- [15] T Dey, A Maljuk, DV Efremov, O Kataeva, S Gass, CGF Blum, F Steckel, D Gruner, T Ritschel, AUB Wolter, *et al.*, “ Ba_2 YrO_6 : a cubic double perovskite material with Ir^{5+} ions,” *Physical Review B* **93**, 014434 (2016).
- [16] Sayantika Bhowal, Santu Baidya, Indra Dasgupta, and Tanusri Saha-Dasgupta, “Breakdown of $j = 0$ nonmagnetic state in d_4 iridate double perovskites: A first-principles study,” *Physical Review B* **92**, 121113 (2015).
- [17] LT Corredor, G Aslan-Cansever, M Sturza, Kaustuv Manna, A Maljuk, S Gass, T Dey, AUB Wolter, Olga Kataeva, A Zimmermann, *et al.*, “Iridium double perovskite Sr_2YrO_6 : A combined structural and specific heat study,” *Physical Review B* **95**, 064418 (2017).
- [18] K Pajskr, P Novák, V Pokorný, J Kolorenč, R Arita, and J Kuneš, “On the possibility of excitonic magnetism in Ir double perovskites,” *Physical Review B* **93**, 035129 (2016).
- [19] Ben Ranjbar, Emily Reynolds, Paula Kayser, Brendan J Kennedy, James R Hester, and Justin A Kimpton, “Structural and magnetic properties of the iridium double perovskites $Ba_{2-x}Sr_xYrO_6$,” *Inorganic chemistry* **54**, 10468–10476 (2015).
- [20] Jiří Chaloupka and Giniyat Khaliullin, “Doping-induced ferromagnetism and possible triplet pairing in d_4 Mott insulators,” *Physical review letters* **116**, 017203 (2016).
- [21] Jasminka Terzic, Hao Zheng, Feng Ye, HD Zhao, P Schlottmann, Lance E De Long, SJ Yuan, and Gang Cao, “Evidence for a low-temperature magnetic ground state in double-perovskite iridates with $Ir^{5+}(5d_4)$ ions,” *Physical Review B* **96**, 064436 (2017).
- [22] Brendan F Phelan, Elizabeth M Seibel, Daniel Badoe Jr, Weiwei Xie, and RJ Cava, “Influence of structural distortions on the Ir magnetism in Ba_2 - Sr - YrO_6 double perovskites,” *Solid State Communications* **236**, 37–40 (2016).
- [23] S Fuchs, T Dey, G Aslan-Cansever, A Maljuk, S Wurmehl, B Büchner, and V Kataev, “Unraveling the nature of magnetism of the $5d_4$ double perovskite Ba_2YrO_6 ,” *Physical review letters* **120**, 237204 (2018).
- [24] Qiang Chen, Chris Svoboda, Qiang Zheng, Brian C Sales, David G Mandrus, HD Zhou, J-S Zhou, D McComb, Mohit Randeria, Nandini Trivedi, *et al.*, “Magnetism out of antisite disorder in the $j = 0$ compound Ba_2YrO_6 ,” *Physical Review B* **96**, 144423 (2017).
- [25] F Hammerath, R Sarkar, S Kamusella, C Baines, H-H Klauss, T Dey, A Maljuk, S Gaß, AUB Wolter, H-J Grafe, *et al.*, “Diluted paramagnetic impurities in nonmagnetic Ba_2YrO_6 ,” *Physical Review B* **96**, 165108 (2017).
- [26] ZY Zhao, S Calder, AA Aczel, MA McGuire, BC Sales, DG Mandrus, G Chen, N Trivedi, HD Zhou, and J-Q Yan, “Fragile singlet ground-state magnetism in the pyrochlore osmates $R_2Os_2O_7$ ($R = Y$ and Ho),” *Physical Review B* **93**, 134426 (2016).
- [27] Klaus K Wolff, Stefano Agrestini, Arata Tanaka, Martin Jansen, and Liu Hao Tjeng, “Comparative study of potentially $jeff = 0$ ground state iridium (v) in $SrLaNiO_6$, $SrLaMgO_6$, and $SrLaZrO_6$,” *Zeitschrift für anorganische und allgemeine Chemie* **643**, 2095–2101 (2017).
- [28] Beluvalli E Prasad, Thomas Doert, Claudia Felser, and Martin Jansen, “On $jeff = 0$ ground state iridates (v): Tracking residual paramagnetism in new Bi_2NiO_6 ,” *Chemistry—A European Journal* **24**, 16762–16765 (2018).
- [29] MA Laguna-Marco, E Arias-Egido, Cristina Piquer, Vera Cuartero, Leyre Hernández-López, Paula Kayser, JA Alonso, JAT Barker, G Fabbris, CA Escanhoela Jr, *et al.*, “Magnetism of Ir^{5+} -based double perovskites: Unraveling its nature and the influence of structure,” *Physical Review B* **101**, 014449 (2020).
- [30] NR Davies, CV Topping, H Jacobsen, AJ Princep, FKK Kirschner, MC Rahn, M Bristow, JG Vale, I Da Silva, PJ Baker, *et al.*, “Evidence for a $jeff = 0$ ground state and defect-induced spin glass behavior in the pyrochlore osmate $Y_2Os_2O_7$,” *Physical Review B* **99**, 174442 (2019).
- [31] Hoshin Gong, Kyoo Kim, Beom Hyun Kim, Bongjae Kim, Junwon Kim, and BI Min, “Is the ground state of $5d_4$ double-perovskite iridate Ba_2YrO_6 magnetic or nonmagnetic?” *Journal of Magnetism and Magnetic Materials* **454**, 66–70 (2018).
- [32] Youwen Long and Yuichi Shimakawa, “Intermetallic charge transfer between a-site Cu and b-site Fe in a-site-ordered double perovskites,” *New Journal of Physics* **12**, 063029 (2010).

- [33] J Hejtmánek, E Šantavá, K Knížek, M Maryško, Z Jiráček, T Naito, H Sasaki, and H Fujishiro, “Metal-insulator transition and the $pr\ 3+/pr\ 4+$ valence shift in $(pr\ 1-y\ y)\ 0.7\ ca\ 0.3\ coo\ 3$,” *Physical Review B* **82**, 165107 (2010).
- [34] Qingdi Zhou, Brendan J Kennedy, Kia S Wallwork, Margaret M Elcombe, Yongjae Lee, and Thomas Vogt, “Temperature and pressure dependent structural studies of the ordered double perovskites $sr_2tbru_1-xirxo_6$,” *Journal of Solid State Chemistry* **178**, 2282–2291 (2005).
- [35] Yoshihiro Doi, Yukio Hinatsu, Ken-ichi Oikawa, Yutaka Shimojo, and Yukio Morii, “Magnetic properties and crystal structures of ordered perovskites $sr_2tbru_1-xirxo_6$,” *Journal of Materials Chemistry* **10**, 1731–1735 (2000).
- [36] Makoto Wakeshima, Yuki Izumiyama, Yoshihiro Doi, and Yukio Hinatsu, “Valence transition in ordered perovskites $ba_2prru_1-xirxo_6$,” *Solid state communications* **120**, 273–278 (2001).
- [37] J Sannigrahi, DT Adroja, C Ritter, W Kockelmann, AD Hillier, KS Knight, AT Boothroyd, M Wakeshima, Y Hinatsu, JFW Mosselmans, *et al.*, “First-order valence transition: Neutron diffraction, inelastic neutron scattering, and x-ray absorption investigations on the double perovskite $ba_2prru_0.9ir_0.1o_6$,” *Physical Review B* **99**, 184440 (2019).
- [38] Qingdi Zhou and Brendan J Kennedy, “Independent structural and valence state transitions in the cation-ordered double perovskites $ba_2-xrxrtb_2o_6$,” *Journal of Solid State Chemistry* **178**, 3589–3594 (2005).
- [39] Makoto Wakeshima, Daijitsu Harada, and Yukio Hinatsu, “Crystal structures and magnetic properties of ordered perovskites ba_2lniro_6 ($ln = \text{lanthanide}$),” *Journal of Materials Chemistry* **10**, 419–422 (2000).
- [40] Daijitsu Harada, Makoto Wakeshima, Yukio Hinatsu, Kenji Ohoyama, and Yasuo Yamaguchi, “Magnetic and neutron diffraction study on iridium (iv) perovskites sr_2lniro_6 ($ln = ce, tb$),” *Journal of Physics: Condensed Matter* **12**, 3229 (2000).
- [41] Daijitsu Harada, Makoto Wakeshima, and Yukio Hinatsu, “The structure and magnetic properties of new iridium (iv) perovskites sr_2lniro_6 ($ln = ce, tb$),” *Journal of Solid State Chemistry* **145**, 356–360 (1999).
- [42] Luuk JP Ament, Michel Van Veenendaal, Thomas P Devereaux, John P Hill, and Jeroen Van Den Brink, “Resonant inelastic x-ray scattering studies of elementary excitations,” *Reviews of Modern Physics* **83**, 705 (2011).
- [43] NE Brese and M O’keeffe, “Bond-valence parameters for solids,” *Acta Crystallographica Section B: Structural Science* **47**, 192–197 (1991).
- [44] AS Wills, “A new protocol for the determination of magnetic structures using simulated annealing and representational analysis (sarah),” *Physica B: Condensed Matter* **276**, 680–681 (2000).
- [45] Philippe Veber, Matias Velázquez, Grégory Gadret, Daniel Rytz, Mark Peltz, and Rodolphe Decourt, “Flux growth at 1230 c of cubic tb_2o_3 single crystals and characterization of their optical and magnetic properties,” *CrystEngComm* **17**, 492–497 (2015).